Earth and Planetary Science Letters 482 (2018) 407–413

Contents lists available at ScienceDirect

Earth and Planetary Science Letters

www.elsevier.com/locate/epsl

Evolution of *b*-value during the seismic cycle: Insights from laboratory experiments on simulated faults

J. Rivière [a,b,*], Z. Lv [c,b], P.A. Johnson [d], C. Marone [b]

[a] University of Grenoble Alpes, ISTerre, F-38000, Grenoble, France
[b] Department of Geosciences, Pennsylvania State University, University Park, PA 16802, USA
[c] State Key Laboratory of Hydroscience and Hydraulic Engineering, Tsinghua University, Beijing 100084, China
[d] Geophysics Group, Los Alamos National Laboratory, MS D446, Los Alamos, NM 87545, USA

ARTICLE INFO

Article history:
Received 13 August 2017
Received in revised form 14 November 2017
Accepted 15 November 2017
Available online xxxx
Editor: P. Shearer

Keywords:
earthquakes
friction
fault
seismic cycle
b-value
acoustic emission

ABSTRACT

We investigate the evolution of the frequency-magnitude *b*-value during stable and unstable frictional sliding experiments. Using a biaxial shear configuration, we record broadband acoustic emissions (AE) while shearing layers of simulated granular fault gouge under normal stresses of 2–8 MPa and shearing velocity of 11 μm/s. AE event amplitude ranges over 3–4 orders of magnitude and we find an inverse correlation between *b* and shear stress. The reduction of *b* occurs systematically as shear stress rises prior to stick–slip failure and indicates a greater proportion of large events when faults are more highly stressed. For quasi-periodic stick–slip events, the temporal evolution of *b* has a characteristic saw-tooth pattern: it slowly drops as shear stress increases and quickly jumps back up at the time of failure. The rate of decrease during the inter-seismic period is independent of normal stress but the average value of *b* decreases systematically with normal stress. For stable sliding, *b* is roughly constant during shear, however it exhibits large variability. During irregular stick–slip, we see a mix of both behaviors: *b* decreases during the interseismic period between events and then remains constant when shear stress stabilizes, until the next event where a co-seismic increase is observed. Our results will help improve seismic hazard assessment and, ultimately, could aid earthquake prediction efforts by providing a process-based understanding of temporal changes in *b*-value during the seismic cycle.

1. Introduction

The long-term goal of predicting earthquakes remains challenging, with progress impeded by a combination of factors that include fault zone structural complexity, heterogeneity in stress state and frictional properties, and a lack of understanding about the weakening and failure processes that occur during earthquake nucleation. One approach has been to use statistical measures of past seismic activity to infer future behaviors and assess seismic hazard (Schorlemmer et al., 2004; Benz et al., 2015; Gulia et al., 2016). The earthquake *b*-value, which describes the frequency-magnitude scaling, has been used for long-term seismic hazard assessment and also as a tool for shorter-term forecasting and studies of earthquake scaling relations (e.g., Davison and Scholz, 1985). Complementary studies have also been conducted in the laboratory, where stresses, displacements and seismic activity can be accurately measured (Scholz, 1968a, 1968b; Lockner et al., 1991; Voisin et al., 2007; Schubnel et al., 2011; Goebel et al., 2013, 2017; Johnson et al., 2013; McLaskey et al., 2014; Kwiatek et al., 2014; McLaskey and Lockner, 2016; Lei et al., 2016; Passelègue et al., 2016; Rouet-Leduc et al., 2017).

Seismic activity is often monitored using the well-known frequency-magnitude relation of Gutenberg and Richter (1944):

$$\log_{10}(N) = a - bM$$

where N is the number of earthquakes larger than magnitude M, a is a measure of the seismic activity and b – referred to as *b*-value – gives insights on the relative scaling of large versus small earthquakes (a larger proportion of large earthquakes lead to a lower *b*-value). There is a rich literature on the relationship between *b*-value, earthquake physics and the scaling laws for seismic sources, e.g., Hanks (1979), Pacheco et al. (1992), Scholz (2002), including works showing that *b*-value correlates with the local differential stress ($\sigma_1 - \sigma_3$) at both laboratory and tectonic scales (Schorlemmer et al., 2005; Spada et al., 2013; Scholz, 2015). These works show that *b*-value is lower at depth and that it decreases with differential stress. Other studies on diverse rock types

* Corresponding author.
E-mail address: jvr5626@psu.edu (J. Rivière).

https://doi.org/10.1016/j.epsl.2017.11.036
0012-821X/

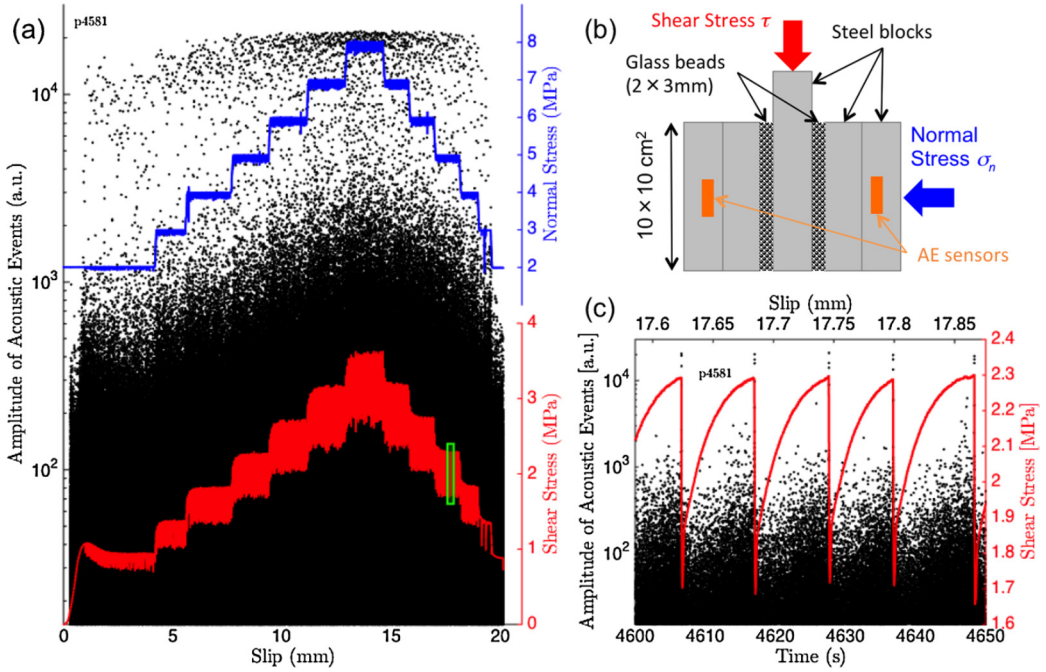

Fig. 1. (a) Data for one complete experiment, showing the imposed normal stress history, the shear stress and AE record during shear. The amplitude A of acoustic emission events (on Channel 1) is shown on a logarithmic scale. **(b)** Experimental Setup. A double direct shear (DDS) configuration is used to shear two granular layers (initial thickness of 3 mm; nominal frictional contact area of 0.01 m^2 at a constant sliding velocity (11 μm/s) and a suite of normal stresses. Two broadband piezoceramics embedded inside steel blocks are placed on each side of the DDS assembly to record acoustic emission taking place inside the layers. **(c)** Details on the stick–slip cycles at a normal load of 5 MPa (green rectangle in **a**), as well as the amplitude of acoustic emission events. (For interpretation of the references to color in this figure legend, the reader is referred to the web version of this article.)

and stress conditions have shown that *b*-value gradually decreases when approaching failure as larger and more numerous foreshocks occur (Scholz, 1968b; Goebel et al., 2013, 2015). There also seems to be a correlation between the magnitude of co-seismic stress drop and the subsequent increase in *b*-value (Goebel et al., 2013).

The purpose of this study is to improve and expand upon experimental observations of the temporal changes in *b*-value that occur during the seismic cycle. Our experiments include 10's to hundreds of stick–slip events that range from periodic to aperiodic, and we study the affect of normal stress on stick–slip recurrence time and temporal changes in *b*-value. Our data provide key physical insights on the processes at play and will improve the ability to interpret temporal changes in *b*-value for seismic data.

2. Experimental setup and protocol

We conduct friction experiments on layers of glass beads in a double-direct shear configuration. Glass beads are of particular interest to monitor seismic activity due to their highly responsive acoustic properties (low attenuation) in comparison to natural gouge. In addition, the use of spherical gouge particles provides a straightforward connection to numerical simulations that can provide useful insights for the underlying micromechanical processes (Morgan, 1999; Morgan and Boettcher, 1999; Abe and Mair, 2005; Mair and Hazzard, 2007; Ferdowsi et al., 2013; Dorostkar et al., 2017).

Our double direct shear (DDS) configuration consists of two granular layers (each 3 mm-thick with nominal contact area of 10×10 cm^2) composed of particles of diameter 100–140 μm sandwiched between three hardened steel forcing blocks (Fig. 1b). The central block is 15-cm high so that the frictional area remains constant throughout shear. The steel blocks have 0.8 mm-deep and 1 mm-spaced teeth perpendicular to the shear direction to prevent sliding along the bounding surface (Frye and Marone, 2002; Mair et al., 2002; Anthony and Marone, 2005; Knuth and Marone, 2007). Cellophane tape is used to maintain the beads in place during sample construction. A thin latex membrane is positioned at the bottom of the sample to prevent loss of material during the experiment. Similarly, four steel guide platens are tightened on the side of the sample to prevent lateral losses.

Normal stress is applied to the nominal frictional area of 0.01 m^2 and maintained by servohydraulic control, while the central steel block is driven down at a constant velocity of 11 μm/s. Horizontal and vertical forces are measured using two strain gauge load cells with resolution of ±10 N, while the corresponding displacements are measured with Direct-Current Displacement Transducers (DCDTs) with ±0.1 μm precision. Two broadband piezoelectric sensors (∼0.02–2 MHz) are embedded within steel blocks that are placed on each side of the sample assembly (Fig. 1b). Both sets of PZTs are epoxied in place at the base of blind holes that are 28 mm in diameter. The piezoceramics – sketched as orange rectangles in Fig. 1b – are 12.7 mm in diameter, 4-mm thick, and 3.18 mm from the face of the side forcing blocks of the DDS assembly. We refer to data from one side as Channel 1 and from the other side as Channel 2. Both sets of PZTs were subject to calibration and testing procedure, and we found negligible differences in the signals.

Forces and displacements are recorded continuously at 1 kHz, while seismic activity is recorded at 4 MHz. All measurements of force and displacement for the DDS configuration are referenced to one layer, assuming symmetric behavior for the two layers. We begin each experiment by applying a 2 MPa-normal load and then wait until the layers compact, creep, and reach a constant thickness. The vertical piston is then driven at constant speed. Shear stress slowly increases and reaches a peak yield strength, after which stick–slip cycles begin (Fig. 1a). We often explore a range of normal stresses during one experiment, although we also conduct experiments at a single normal stress to assess the role of shear displacement. The focus below is on results from a typical

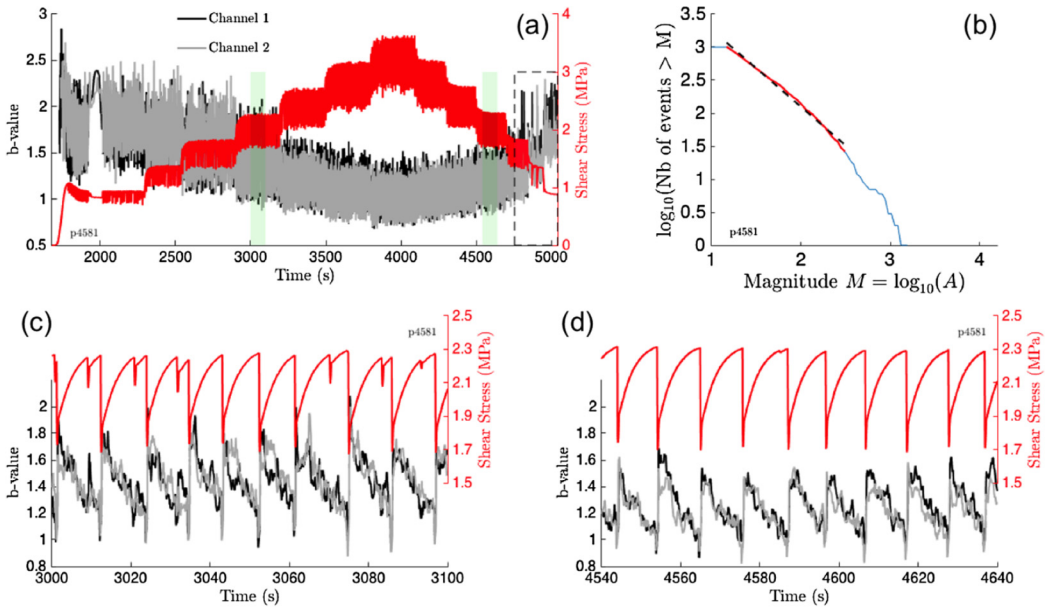

Fig. 2. Evaluation of the AE frequency-magnitude parameter b and its evolution over a complete experiment. **(a)** Shear stress and b-value as a function of time during shear for events recorded on each PZT. The two green rectangles correspond to two portions detailed in (c) and (d). The dashed black rectangle corresponds to a portion detailed in Fig. 3. Note the consistency of the b-values computed for each acoustic channel. **(b)** Typical frequency-magnitude plot made with a 1000-event window length. Magnitude M is arbitrarily defined as the log of the acoustic event amplitude. Values b are computed over the magnitude range [1.18–2.5]. Within that range, the coefficient of determination r^2 for the entire set of b-values is found larger than 0.9, with a vast majority above 0.95 (see supplementary material for further details). **(c)** Details on the evolution of b and shear stress at 5 MPa normal stress during the phase of increasing normal stress (left green rectangle in Panel a). Note the consistency of aperiodic stick–slip failure events and the corresponding signature in the b-values. **(d)** Details on the evolution of b and shear stress at 5 MPa during the phase of decreasing normal stress (right green rectangle in Panel a). Note the periodic nature of the stick–slip failure events and the corresponding signature in the b-value data. (For interpretation of the references to color in this figure legend, the reader is referred to the web version of this article.)

experiment. The full suite of experiments for this study numbered over 25. For tests with multiple normal stresses, we start at one value and then impose 1 MPa-stepwise increases from 2 to 8 MPa, followed by stepwise decreases back to 2 MPa (Fig. 1).

3. Results

In a typical run (Fig. 1) we detect over 4 million events per channel over ∼1.4 hour and 20-mm of imposed shear slip. AE event amplitudes (A) span over 3 orders of magnitude (black dots in Fig. 1a–c). The seismic magnitude in Equation (1) is arbitrarily defined as $M = \log_{10}(A)$, with A expressed in units of bits. In Fig. 1c, a detailed view on a few seismic cycles at 5-MPa normal load shows the evolution of shear stress as well as the magnitude of seismic events for Channel 1. A general increase in seismic activity can be seen as failure approaches (i.e., larger and more numerous events). Only events for channel 1 are represented in Fig. 1a–c for clarity, and as described below, both channels lead to similar observations. For each acoustic sensor, we compute the b-value using sliding windows that contain a constant number of seismic events (1000) and apply an overlap of 900 events (the window is shifted by 100 events each time, i.e., ∼90% overlap). We conducted this analysis with various window sizes and overlaps to check consistency of the results and found slight variations; however, the general conclusions of this work are not affected by the choice of these parameters.

Fig. 2a shows the general evolution of b-value for an entire experiment. Fig. 2b shows a typical frequency-magnitude plot for one particular window (1000 events). The magnitude range over which b-values are computed is $M = [1.18–2.5]$. The lower bound 1.18 corresponds to a threshold chosen above the noise level (i.e., $A = 15$ bits) and corresponds to the 'catalog completeness' value of seismic data, while the upper bound 2.5 is chosen such that a linear fit remains appropriate ($r^2 > 0.9$) (see supplementary material for further details). In Fig. 2a, the inverse correlation between b-value and normal stress is consistent with the idea that larger events are proportionally more numerous on highly stressed faults, leading to lower b-values. Figs. 2c and 2d show details on the b-value evolution during both aperiodic and periodic stick–slip sequences. These data represent shear stress at 5-MPa normal load during the time of increasing and decreasing normal stresses, respectively (shown as green, shaded areas in Fig. 2a). In both cases, we observe a gradual decrease in b-value as shear stress increases and a sudden b-value increase at the time of stick–slip failure. Small stress drops occurring during irregular seismic cycles (Fig. 2c) also cause an increase in b-value, although these are often near or within the noise associated with the evolution of b.

Fig. 3 shows a detailed view on the last downward normal stress steps, from 4 to 2 MPa, shown in Fig. 2a. This section shows how b evolves as the fault transitions from quasi-periodic stick–slips to stable-sliding conditions. At 4 MPa, b ranges between ∼1 and ∼1.8 with a behavior similar to that observed in Fig. 2d, typical of regular stick–slips. On the other hand, at 2 MPa, b is larger on average (1.4–2.2) and becomes rather constant, with a slight difference between the two channels. At 3 MPa, a mixture of both behaviors can be observed: b increases rapidly during slip events, gradually decreases during the reloading portion of the cycle and finally remains constant during creep.

In Fig. 4, we show the b-value averaged over each normal stress step as a function of normal stress for both channels. We clearly see the inverse correlation between b and normal stress, as also shown in Fig. 2a. We find that b is slightly larger during the step-up phase compared to the step-down phase, leading to a small hysteresis. Larger b-values during the step-up phase may be due to the fact that (i) seismic cycles are more irregular, and (ii) shear stress is on average slightly smaller (i.e. slightly smaller friction coefficient). We believe the hysteretic effects are due to the gradual gouge layer thinning as the experiment proceeds.

To further relate our observations to earthquake faults we focus on the stick–slip regime and investigate how b-value evolves as

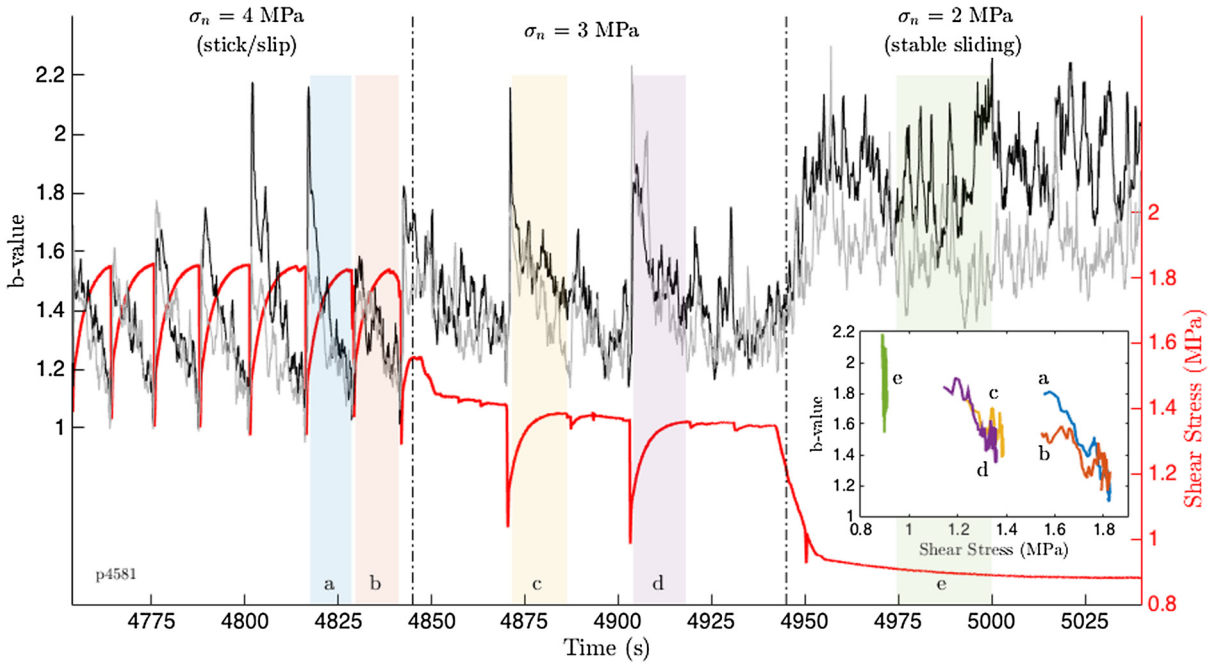

Fig. 3. Shear stress and *b*-value evolution as a function of time during the transition between stick–slip, at 4 MPa, and stable sliding at 2 MPa. Periodic stick–slip events at 4 MPa become irregular as shear stress decreases to 3 MPa and then shear becomes stable at 2 MPa. The *b*-value data show a tightly correlated evolution during this transition, from the systematic decrease as a function of time during the seismic cycle (at 4 MPa) to stable but highly variable behavior during steady frictional sliding. These data are from the region indicated by the dashed black rectangle in Fig. 2. The inset shows *b*-value as a function of shear stress for five specific portions encompassing the three regimes (regular stick/slip, irregular stick/slip, stable sliding).

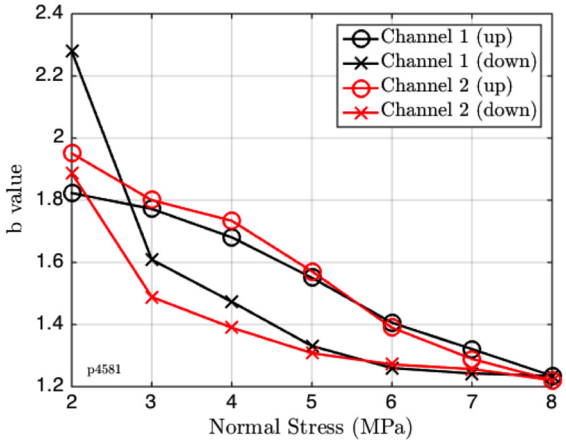

Fig. 4. Frequency-magnitude *b*-value as function of normal stress for the experiment shown in Fig. 1. These data are averages at each normal stress during the phase of increasing (circles) and decreasing (x'es) normal stress. Note the inverse correlation between *b* and stress and the hysteresis associated with increasing and decreasing normal stress.

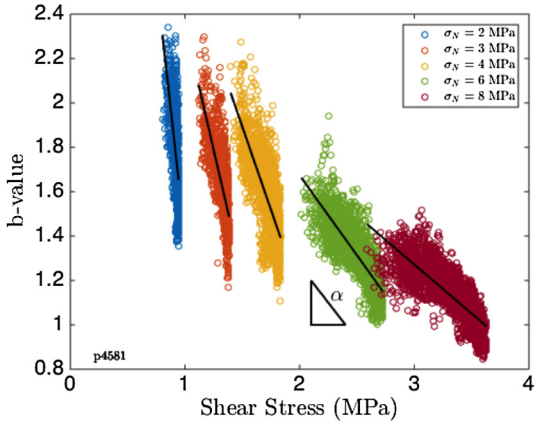

Fig. 5. *b*-value evolution as a function of shear stress for all seismic cycles at 2, 3, 4, 6 and 8 MPa-normal load during the phase of increasing normal stress. A similar behavior is found at all steps and during the downward phase. Only data for five normal stresses are shown for clarity. Black lines show best-fit slope, α, of the evolution of *b* during shear.

shear stress increases following each slip event. In Fig. 5, we show such evolution for five normal stresses (2, 3, 4, 6 and 8 MPa) during the phase of increasing normal stress. We focus on these five values for clarity: similar behavior is seen at all normal stresses and during the phase of decreasing normal stress. Several observations can be made. First, the range in shear stress increases with normal stress, indicative of larger shear stress drops at larger normal stresses. On the other hand, the range in *b*-value is larger at low normal stress: it spans the range 1.3 to 2.3 at 2 MPa, while only ~0.8 to 1.5 at 8 MPa. When computing the slope α (in MPa^{-1}) at each normal stress step, one clearly sees how α increases (the absolute value of α decreases). In Fig. 6, we report *b*-value as a function of friction, that is shear stress divided by normal stress. One can observe an overall small decrease in friction during the first normal stress steps (up to about 0.01 when normal stress is stepped up from 2 to 3 MPa), likely due to initial rearrangement of the layers. This is corroborated by the observation of larger aperiodicity in the seismic cycles during these first normal stress steps (as shown in Fig. 2c), leading to larger scatter in *b*-value. Similar data are reported in Fig. 7a, with the difference that shear stress is normalized to the maximum shear stress (shear stress preceding failure) for each seismic cycle (Scholz, 1968b). We capture the evolution by computing the slope (β) at each normal stress step. Finally, in Fig. 7b, *b*-value as a function of time preceding failure is reported for each seismic cycle and the slope δ (s^{-1}) is computed for each normal stress step. Slopes α, β and δ are reported in Fig. 8 as a function of normal stress for the two AE channels. We find that α and β increase with normal stress, with similar results for both channels. Furthermore, despite complex behaviors such as irregular stick–slip cycles during the upward phase (leading to hysteresis in Fig. 4), no major difference can be seen

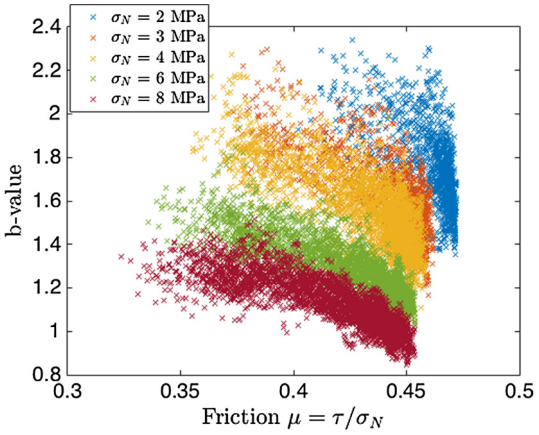

Fig. 6. b-value evolution as a function of friction $\mu = \tau/\sigma_n$ for all seismic cycles at 2, 3, 4, 6 and 8 MPa-normal load during the phase of increasing normal stress. Only data for five normal stresses are shown for clarity.

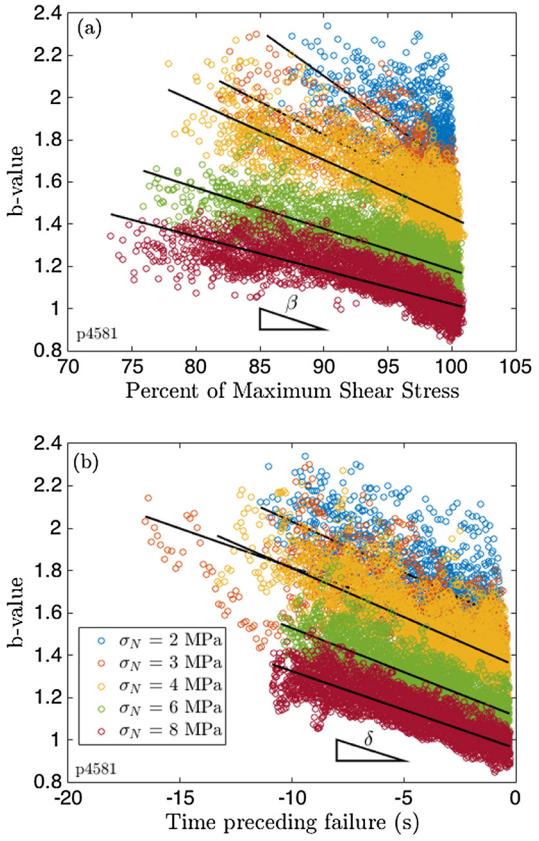

Fig. 7. (a) Same as Fig. 5 except that shear stress is normalized to the maximum shear stress for each stick–slip failure event. The b-value decreases systematically with increasing normal stress and as a function of normalized shear stress during each seismic cycle. (b) b-value evolution as a function of time for all seismic cycles at 2, 3, 4, 6 and 8 MPa-normal load during the phase of increasing normal stress. Note that b-value decreases linearly with time prior to failure. The evolution of the slope δ is displayed in Fig. 8c.

between the upward and downward phases for α and β. As far as the slope δ is concerned, no clear evolution with normal stress can be seen, suggesting that over the stress range explored, the "time to failure" seems independent of the stress conditions on the fault.

4. Discussion

When comparing b-values and stress conditions across many fault types and tectonic regions, Scholz (2015) found the following inverse correlation between b-value and differential stress: $b = 1.23 - 0.0012(\sigma_1 - \sigma_3)$ with $(\sigma_1 - \sigma_3)$ expressed in MPa. If differential stress is replaced by shear stress using $\tau \sim (\sigma_1 - \sigma_3)/2$, the slope 0.0012 becomes 0.0024 MPa^{-1} and can be compared to the $|\alpha|$ values we measured (Fig. 8). Our measurements of $|\alpha|$ range from 4 to 0.3 MPa^{-1}, which is two or three orders of magnitude larger than the field-based estimates. However, the stress range covered in our work ($\tau = 0.8$–3.6 MPa) is also one or two orders of magnitude lower than for the field data (~10–250 MPa). Further, our observations show that $|\alpha|$ drops by an order of magnitude (from 4 down to 0.3) when stress increases by less than an order of magnitude. Therefore, in the plausible case that $|\alpha|$ keeps dropping with increasing stress, there could be a quantitative agreement between the lab and field observations.

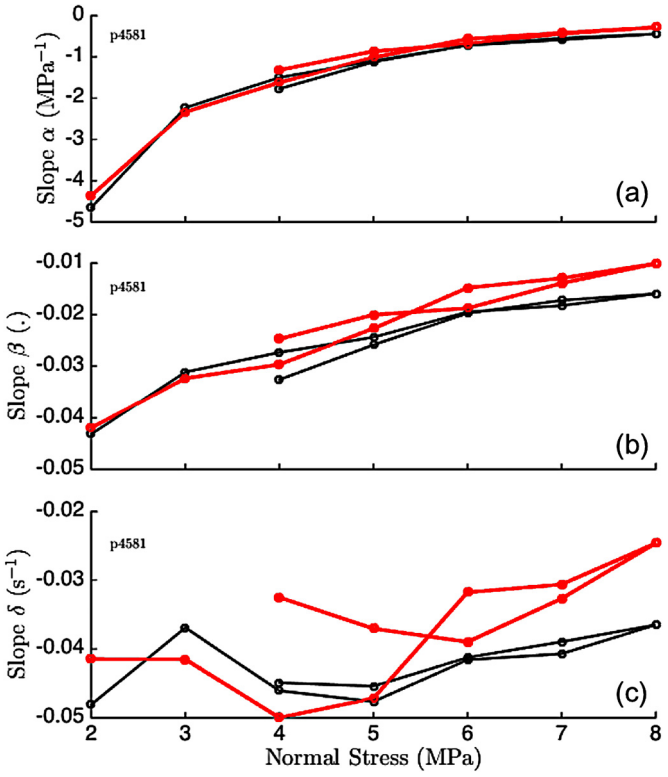

Fig. 8. Evolution of the functional relationship between b-value and shear stress (a), normalized shear stress (b) and time to failure (c).

As shown in Fig. 7b, we find that b-value decreases continuously with time to failure, with a rate δ that is rather independent of stress (Fig. 8c). Such behavior suggests that the processes leading to time failure do not vary strongly during the seismic cycle, and that observations made at different stress levels might be directly compared.

Overall, the physical description of fault zones is complex and can be described within different frameworks (Ben-Zion and Sammis, 2003). Stick/slip behavior in simple glass bead layers occurs at relatively low stresses, when beads do not break, and for narrow particle size distribution (Mair et al., 2002). Such stick/slips are often described in terms of formation and breakage of force chains during loading and creeping portions of the seismic cycle respectively (Nasuno et al., 1997, 1998; Mair et al., 2002; Majmudar and Behringer, 2005; Daniels and Hayman, 2008; Johnson et al., 2008). The DEM simulations show correlations to kinetic and potential energy indicating grain mobilization in the gouge layer at the time of slip but less during the inter-event period, possibly supporting the force chain concept (Ferdowsi et al., 2013; Dorostkar et al., 2017). At stresses where particles can break (those encountered in natural faults), fault zones are often described in terms of frac-

tal structures with no characteristic scales (Sammis et al., 1987; Marone and Scholz, 1989; Amitrano, 2012). At the tectonic scale, rather than a steady decrease during the inter-seismic period, *b*-value exhibits rather larger variability, in the rare cases where it has been measured (Schorlemmer et al., 2004, 2005; Spada et al., 2013; Benz et al., 2015; Petersen et al., 2015), including examples where it decreases, and some where it increases, prior to failure. In one recent study, Gulia et al. (2016) found a pronounced drop in *b*-value a few weeks prior to earthquake failure. The differences between tectonic faults and lab-scale experiments is likely due to greater complexity of geological faults, including a large number of interacting faults, however future work must consider other possible explanations.

Despite differences in stress and fault nature/composition, our results show striking similarities with observations made in naturally developed laboratory faults in rocks (Scholz, 1968b; Amitrano, 2003; Goebel et al., 2013). In both cases, *b*-value is found to progressively decrease until failure is reached. Seismic stress drops are then accompanied with sudden *b*-value increases. The overall similarity between results in glass beads and natural rocks suggests that the use of glass bead layers at relatively low stresses is relevant for seismic studies of *b*-value.

5. Conclusions

We study the temporal evolution of *b*-values along 275 seismic cycles in glass bead layers and under various stress conditions. Our results complement the observations from previous laboratory studies (Scholz, 1968b; Lei, 2003; Lei et al., 2003; Thompson et al., 2005; Michlmayr et al., 2012; Goebel et al., 2013; Johnson et al., 2013; Kwiatek et al., 2014) as well as field studies (Schorlemmer et al., 2005; Benz et al., 2015; Scholz, 2015; Petersen et al., 2015; Gulia et al., 2016). We find that *b*-value continuously decreases with time as failure approaches, with a rate rather independent of normal stress. An inverse correlation between *b*-value and stress is also observed that is qualitatively consistent with literature. A comparison with equivalent results at the Earth's scale shows some quantitative discrepancies that might be explained by differences in stress range.

Acknowledgements

This work was supported by a Marie-Curie Fellowship to JR (Award Number 655833), and grants from the DOE-Geothermal program, the NSF (1547441 and 1520760), and the USGS/NEHRP (Award Numbers G16AP00028 & G16AP00027) to CJM. PAJ acknowledges DOE Geothermal and Institutional Support (LDRD) at Los Alamos National Laboratory.

Appendix A. Supplementary material

Supplementary material related to this article can be found online at https://doi.org/10.1016/j.epsl.2017.11.036.

References

Abe, S., Mair, K., 2005. Grain fracture in 3D numerical simulations of granular shear. Geophys. Res. Lett. 32, L05305.

Amitrano, D., 2003. Brittle–ductile transition and associated seismicity: experimental and numerical studies and relationship with the *b* value. J. Geophys. Res. 108, 1–15.

Amitrano, D., 2012. Variability in the power-law distributions of rupture events. Eur. Phys. J. Spec. Top. 205, 199–215.

Anthony, J.L., Marone, C., 2005. Influence of particle characteristics on granular friction. J. Geophys. Res., Solid Earth 110, B08409.

Benz, H.M., McMahon, N.D., Aster, R.C., McNamara, D.E., Harris, D.B., 2015. Hundreds of earthquakes per day: the 2014 Guthrie, Oklahoma, earthquake sequence. Seismol. Res. Lett. 86, 1318–1325.

Ben-Zion, Y., Sammis, C.G., 2003. Characterization of fault zones. Pure Appl. Geophys. 160, 677–715.

Daniels, K.E., Hayman, N.W., 2008. Force chains in seismogenic faults visualized with photoelastic granular shear experiments 113, 1–13.

Davison, F.C., Scholz, C.H., 1985. Frequency-moment distribution of earthquakes in the Aleutian Arc: a test of the characteristic earthquake model. Bull. Seismol. Soc. Am. 75, 1349–1361.

Dorostkar, O., Guyer, R.A., Johnson, P.A., Marone, C., Carmeliet, J., 2017. On the role of fluids in stick–slip dynamics of saturated granular fault gouge using a coupled computational fluid dynamics-discrete element approach: stick–slip in saturated fault gouge. J. Geophys. Res., Solid Earth 122, 3689–3700.

Ferdowsi, B., Griffa, M., Guyer, R.A., Johnson, P.A., Marone, C., Carmeliet, J., 2013. Microslips as precursors of large slip events in the stick–slip dynamics of sheared granular layers: a discrete element model analysis: 3-D DEM modeling of stick slip. Geophys. Res. Lett. 40, 4194–4198.

Frye, K.M., Marone, C., 2002. Effect of humidity on granular friction at room temperature: effect of humidity on granular friction. J. Geophys. Res., Solid Earth 107, 1–13. ETG11.

Goebel, T.H.W., Schorlemmer, D., Becker, T.W., Dresen, G., Sammis, C.G., 2013. Acoustic emissions document stress changes over many seismic cycles in stick–slip experiments. Geophys. Res. Lett. 40, 2049–2054.

Goebel, T.H.W., Sammis, C.G., Becker, T.W., Dresen, G., Schorlemmer, D., 2015. A comparison of seismicity characteristics and fault structure between stick–slip experiments and nature. Pure Appl. Geophys. 172, 2247–2264.

Goebel, T.H.W., Kwiatek, G., Becker, T.W., Brodsky, E.E., Dresen, G., 2017. What allows seismic events to grow big?: insights from *b*-value and fault roughness analysis in laboratory stick–slip experiments. Geology 45, 815–818.

Gulia, L., Tormann, T., Wiemer, S., Herrmann, M., Seif, S., 2016. Short-term probabilistic earthquake risk assessment considering time-dependent *b* values: time-dependent *b* value and risk. Geophys. Res. Lett. 43, 1100–1108.

Gutenberg, B., Richter, C.F., 1944. Frequency of earthquakes in California. Bull. Seismol. Soc. Am. 34, 185–188.

Hanks, T.C., 1979. Estimation of high-frequency strong ground motion. J. Geophys. Res. 84, 2235–2242.

Johnson, P.A., Savage, H.M., Knuth, M., Gomberg, J., Marone, C., 2008. Effects of acoustic waves on stick–slip in granular media and implications for earthquakes. Nature 451, 57–60.

Johnson, P.A., Ferdowsi, B., Kaproth, B.M., Scuderi, M., Griffa, M., Carmeliet, J., Guyer, R.A., Le Bas, P.Y., Trugman, D.T., Marone, C., 2013. Acoustic emission and microslip precursors to stick–slip failure in sheared granular material. Geophys. Res. Lett. 40, 5627–5631.

Knuth, M., Marone, C., 2007. Friction of sheared granular layers: role of particle dimensionality, surface roughness, and material properties. Geochem. Geophys. Geosyst. 8, Q03012.

Kwiatek, G., Goebel, T.H.W., Dresen, G., 2014. Seismic moment tensor and *b* value variations over successive seismic cycles in laboratory stick–slip experiments. Geophys. Res. Lett. 41, 5838–5846.

Lei, X., 2003. How do asperities fracture? An experimental study of unbroken asperities. Earth Planet. Sci. Lett. 213, 347–359.

Lei, X., Kusunose, K., Satoh, T., Nishizawa, O., 2003. The hierarchical rupture process of a fault: an experimental study. Phys. Earth Planet. Inter. 137, 213–228.

Lei, X., Funatsu, T., Ma, S., Liu, L., 2016. A laboratory acoustic emission experiment and numerical simulation of rock fracture driven by a high-pressure fluid source. J. Rock Mech. Geotech. Eng. 8, 27–34.

Lockner, D.A., Byerlee, J.D., et al., 1991. Quasi-static fault growth and shear fracture energy in granite. Nature (London) 350, 39.

Mair, K., Hazzard, J.F., 2007. Nature of stress accommodation in sheared granular material: insights from 3D numerical modeling. Earth Planet. Sci. Lett. 259, 469–485.

Mair, K., Frye, K.M., Marone, C., 2002. Influence of grain characteristics on the friction of granular shear zones: grain shape influence on friction. J. Geophys. Res., Solid Earth 107, 1–9. ECV4.

Majmudar, T.S., Behringer, R.P., 2005. Contact force measurements and stress-induced anisotropy in granular materials. Nature 435, 1079–1082.

Marone, C., Scholz, C.H., 1989. Particle-size distribution and microstructures within simulated fault gouge. J. Struct. Geol. 11, 799–814.

McLaskey, G.C., Lockner, D.A., 2016. Calibrated acoustic emission system records M −3.5 to M −8 events generated on a saw-cut granite sample. Rock Mech. Rock Eng. 49, 4527–4536.

McLaskey, G.C., Kilgore, B.D., Lockner, D.A., Beeler, N.M., 2014. Laboratory generated M 6 earthquakes. Pure Appl. Geophys. 171, 2601–2615.

Michlmayr, G., Cohen, D., Or, D., 2012. Sources and characteristics of acoustic emissions from mechanically stressed geologic granular media – a review. Earth-Sci. Rev. 112, 97–114.

Morgan, J.K., 1999. Numerical simulations of granular shear zones using the distinct element method: 2. Effects of particle size distribution and interparticle friction on mechanical behavior. J. Geophys. Res., Solid Earth 104, 2721–2732.

Morgan, J.K., Boettcher, M.S., 1999. Numerical simulations of granular shear zones using the distinct element method: 1. Shear zone kinematics and the micromechanics of localization. J. Geophys. Res., Solid Earth 104, 2703–2719.

Nasuno, S., Kudrolli, A., Gollub, J.P., 1997. Friction in granular layers: hysteresis and precursors. Phys. Rev. Lett. 79, 949.

Nasuno, S., Kudrolli, A., Bak, A., Gollub, J.P., 1998. Time-resolved studies of stick–slip friction in sheared granular layers. Phys. Rev. E 58, 2161.

Pacheco, J.F., Scholz, C.H., Sykes, L.R., 1992. Changes in frequency–size relationship from small to large earthquakes. Nature 355, 71–73.

Passelègue, F.X., Schubnel, A., Nielsen, S., Bhat, H.S., Deldicque, D., Madariaga, R., 2016. Dynamic rupture processes inferred from laboratory microearthquakes: dynamic processes of stick–slip. J. Geophys. Res., Solid Earth 121, 4343–4365.

Petersen, M.D., Mueller, C.S., Moschetti, M.P., Hoover, S.M., Rubinstein, J.L., Llenos, A.L., Michael, A.J., Ellsworth, W.L., McGarr, A.F., Holland, A.A., 2015. Incorporating Induced Seismicity in the 2014 United States National Seismic Hazard Model: Results of 2014 Workshop and Sensitivity Studies. US Department of the Interior, US Geological Survey.

Rouet-Leduc, B., Hulbert, C., Bolton, D.C., Ren, C.X., Marone, C., Guyer, R.A., Johnson, P.A., 2017. Fault friction constitutive law derived from continuous acoustic emissions by machine learning. arXiv preprint arXiv:1710.04172.

Sammis, C., King, G., Biegel, R., 1987. The kinematics of gouge deformation. Pure Appl. Geophys. 125, 777–812.

Scholz, C.H., 1968a. Microfracturing and the inelastic deformation of rock in compression. J. Geophys. Res. 73, 1417.

Scholz, C.H., 1968b. The frequency-magnitude relation of microfracturing in rock and its relation to earthquakes. Bull. Seismol. Soc. Am. 58, 399–415.

Scholz, C.H., 2002. The Mechanics of Earthquakes and Faulting. Cambridge University Press.

Scholz, C.H., 2015. On the stress dependence of the earthquake b value. Geophys. Res. Lett. 42, 1399–1402.

Schorlemmer, D., Wiemer, S., Wyss, M., 2004. Earthquake statistics at Parkfield: 1. Stationarity of b values. J. Geophys. Res. B, Solid Earth 109, 1–17.

Schorlemmer, D., Wiemer, S., Wyss, M., 2005. Variations in earthquake-size distribution across different stress regimes. Nature 437, 539–542.

Schubnel, A., Nielsen, S., Taddeucci, J., Vinciguerra, S., Rao, S., 2011. Photo-acoustic study of subshear and supershear ruptures in the laboratory. Earth Planet. Sci. Lett. 308, 424–432.

Spada, M., Tormann, T., Wiemer, S., Enescu, B., 2013. Generic dependence of the frequency-size distribution of earthquakes on depth and its relation to the strength profile of the crust. Geophys. Res. Lett. 40, 709–714.

Thompson, B.D., Young, R.P., Lockner, D.A., 2005. Observations of premonitory acoustic emission and slip nucleation during a stick slip experiment in smooth faulted Westerly granite. Geophys. Res. Lett. 32, 1–4.

Voisin, C., Renard, F., Grasso, J.-R., 2007. Long term friction: from stick–slip to stable sliding. Geophys. Res. Lett. 34, L13301.